The EMBO Journal (2011) 30, 1852–1863 | © 2011 European Molecular Biology Organization | All Rights Reserved 0261-4189/11
www.embojournal.org

THE EMBO JOURNAL

Two types of chloride transporters are required for $GABA_A$ receptor-mediated inhibition in *C. elegans*

Andrew Bellemer[1,3], Taku Hirata[2], Michael F Romero[2] and Michael R Koelle[1,*]

[1]Department of Molecular Biophysics and Biochemistry, Yale University School of Medicine, New Haven, CT, USA and [2]Department of Physiology and Biomedical Engineering, Mayo Clinic College of Medicine, Rochester, MN, USA

Chloride influx through GABA-gated Cl^- channels, the principal mechanism for inhibiting neural activity in the brain, requires a Cl^- gradient established in part by K^+–Cl^- cotransporters (KCCs). We screened for *Caenorhabditis elegans* mutants defective for inhibitory neurotransmission and identified mutations in ABTS-1, a Na^+-driven Cl^-–HCO_3^- exchanger that extrudes chloride from cells, like KCC-2, but also alkalinizes them. While animals lacking ABTS-1 or the K^+–Cl^- cotransporter KCC-2 display only mild behavioural defects, animals lacking both Cl^- extruders are paralyzed. This is apparently due to severe disruption of the cellular Cl^- gradient such that Cl^- flow through GABA-gated channels is reversed and excites rather than inhibits cells. Neuronal expression of both transporters is upregulated during synapse development, and ABTS-1 expression further increases in KCC-2 mutants, suggesting regulation of these transporters is coordinated to control the cellular Cl^- gradient. Our results show that Na^+-driven Cl^-–HCO_3^- exchangers function with KCCs in generating the cellular chloride gradient and suggest a mechanism for the close tie between pH and excitability in the brain.

The EMBO Journal (2011) **30,** 1852–1863. doi:10.1038/emboj.2011.83; Published online 22 March 2011
Subject Categories: neuroscience
Keywords: *C. elegans*; chloride; GABA; transporter

Introduction

GABA is the primary inhibitory neurotransmitter in the mammalian brain (Mody *et al*, 1994). Cl^- influx through $GABA_A$ receptors results in neuronal hyperpolarization and inhibition. This response depends on maintenance of a relatively low intracellular Cl^- concentration, resulting in a Cl^- reversal potential more negative than the cell's resting membrane potential (Farrant and Kaila, 2007). Many immature neurons maintain high intracellular Cl^- levels, resulting in a Cl^- reversal potential more positive than the cell's resting potential, so that GABA can elicit Cl^- efflux and an excitatory response (Ben-Ari, 2002; Blaesse *et al*, 2009). Thus, neurons regulate intracellular Cl^- levels to control the magnitude and polarity of the effects of GABA, and this in turn has been shown to powerfully affect neural development and activity (Fiumelli *et al*, 2005; Akerman and Cline, 2006). Understanding this type of 'ionic plasticity' (Rivera *et al*, 2005) requires understanding which transporters control intracellular Cl^- levels.

Multiple transporters move Cl^- across the plasma membrane. The most extensively studied are the Cl^--extruding K^+–Cl^- cotransporter KCC2 and the Cl^--accumulating Na^+–K^+–$2Cl^-$ cotransporter NKCC1 (Blaesse *et al*, 2009). The excitatory effect of GABA on immature hippocampal and cortical neurons is due in part to their low KCC2 expression and high NKCC1 expression. GABA becomes inhibitory as neurons upregulate expression of KCC2 and downregulate expression of NKCC1 (Rivera *et al*, 1999; Yamada *et al*, 2004; Akerman and Cline, 2006). However, KCC2 is apparently not the sole Cl^- extruder (Rivera *et al*, 1999; Gulacsi *et al*, 2003). Na^+-driven Cl^-–HCO_3^- exchangers (also known as Na^+-driven anion exchangers, or NDAEs) can extrude Cl^- and could contribute to the cellular Cl^- gradient and hyperpolarizing GABA action (Gulacsi *et al*, 2003; Kim and Trussell, 2009). However, to date no specific transporter of this type has been shown to have such a role.

The SLC4 family of ion transporters includes multiple Cl^-–HCO_3^- exchangers (Romero *et al*, 2004). Among these, human and squid NDCBE and *Drosophila* NDAE1 have been shown to function as NDAEs that extrude Cl^- (Romero *et al*, 2000; Grichtchenko *et al*, 2001; Virkki *et al*, 2003). Despite expression of NDCBE in mammalian neurons and its characterized role in regulating neuronal intracellular pH (Schwiening and Boron, 1994; Grichtchenko *et al*, 2001; Chen *et al*, 2008a, b), its role in regulating neuronal intracellular Cl^- homeostasis has not been fully investigated.

The nematode *Caenorhabditis elegans* has been developed as a model organism for genetic analysis of GABAergic neurotransmission (Jorgensen, 2005). *C. elegans* possesses 19 GABAergic motor neurons that synapse on the body wall muscles (BWMs) to promote hyperpolarization and lengthening of muscles contralateral to contracting muscles, producing sinusoidal body bends and coordinated locomotion (McIntire *et al*, 1993b). UNC-49 is the *C. elegans* $GABA_A$ receptor homologue (Bamber *et al*, 1999; Richmond and Jorgensen, 1999). UNC-49 function is required in the BWMs to generate coordinated body bends (McIntire *et al*, 1993a, b; Bamber *et al*, 1999).

More recently, *C. elegans* has been established as a model system in which to identify Cl^- transporters that control GABA signalling. *C. elegans* egg-laying behaviour can be blocked by inactivating the hermaphrodite-specific neurons (HSNs) with a mutation in the putative transmembrane

*Corresponding author. Department of Molecular Biophysics and Biochemistry, Yale University School of Medicine, 333 Cedar Street, SHM CE30, New Haven, CT 06520-8024, USA. Tel.: +1 203 737 2271; Fax: +1 203 785 6404; E-mail: michael.koelle@yale.edu
[3]Present address: Department of Anesthesiology, Duke University Medical Center, Durham, NC 27710, USA

Received: 7 December 2010; accepted: 22 February 2011; published online: 22 March 2011

 ©2011 European Molecular Biology Organization

receptor EGL-47 (Moresco and Koelle, 2004). Suppressor mutations that reactivate the HSNs to allow egg laying to occur identify genes required for inhibitory signalling by GABA, including the gene encoding the K^+–Cl^- cotransporter KCC-2 (Tanis *et al*, 2009). In this work, we have used this screening strategy to identify the Na^+-driven Cl^-–HCO_3^- exchanger ABTS-1 and show that it functions partially redundantly with KCC-2 to control GABAergic signalling in *C. elegans* neurons and muscles.

Results

Mutations in abts-1 suppress egl-47(dm) to reactivate egg laying

Wild-type animals retain 13.1 ± 0.9 eggs *in utero* (Figure 1A), while *egl-47(dm)* mutants fail to lay eggs and thus retain a far larger number, 57.5 ± 2.7 (Figure 1B). More strikingly, wild-type young adults lay many eggs through the first ~12 h of adulthood (70.5 ± 4.4 eggs per pool of five animals assayed), while we have never observed a young adult *egl-47(dm)* animal lay an egg (Figure 1D). Thus, *egl-47(dm)* animals provided an exquisitely clean background in which we were able to identify suppressor mutations that restore HSN activity to reactivate egg laying.

We used the *egl-47(dm)* suppressor screen to identify the *vs145* suppressor mutation, which strongly reactivated egg laying in an *egl-47(dm)* background (Figure 1C and D). We mapped and cloned *vs145* and discovered a mutation in the anion bicarbonate transporter gene, *abts-1*, which encodes a protein similar to mammalian HCO_3^- transporters of the SLC4 family (Sherman *et al*, 2005). The *vs145* mutation results in the substitution of an arginine for a glycine residue within a predicted transmembrane helix (Figure 3A). We obtained a deletion mutation *ok1566* that is a putative null since it removes sequences encoding all of one and parts of two other predicted transmembrane helices. Because *vs145* and *ok1566* are phenotypically similar (Figure 1D and E; data not shown), *vs145* appears to be a strong loss-of-function mutation. Both the *vs145* and *ok1566* alleles restored egg laying in *egl-47(dm)* young adults. The double mutants *abts-1(vs145); egl-47(dm)* and *abts-1(ok1566); egl-47(dm)* (Figure 1C) retained only 7.3 ± 1.2 and 7.3 ± 0.8 eggs *in utero*, respectively, compared with the 57.5 ± 2.7 eggs retained by *egl-47(dm)* single mutants (Figure 1B). As young adults, the double mutants *abts-1(vs145); egl-47(dm)* and *abts-1(ok1566); egl-47(dm)* laid 20.3 ± 4.0 and 30.2 ± 4.5, respectively, compared with the 0.0 ± 0.0 eggs laid by *egl-47(dm)* single mutants (Figure 1D). Thus, mutations in *abts-1* suppress *egl-47(dm)* by reactivating egg laying in young adults.

Loss of abts-1 causes the egl-47(dm) mutation to stimulate rather than inhibit egg laying

abts-1 mutations are similar to *kcc-2* mutations in that both show the same remarkable interaction with *egl-47(dm)*. While *egl-47(dm)* strongly inhibits egg laying in a wild-type genetic background, it instead stimulates egg laying in a *kcc-2* mutant background such that *kcc-2; egl-47(dm)* mutants lay eggs at a much higher rate than do wild-type animals (Tanis *et al*, 2009). The stimulatory effect of the *egl-47(dm)* mutation on function of HSNs lacking KCC-2 may be analogous to the excitatory action of GABA on immature mammalian neurons that do not express KCC2 (Rivera *et al*, 1999).

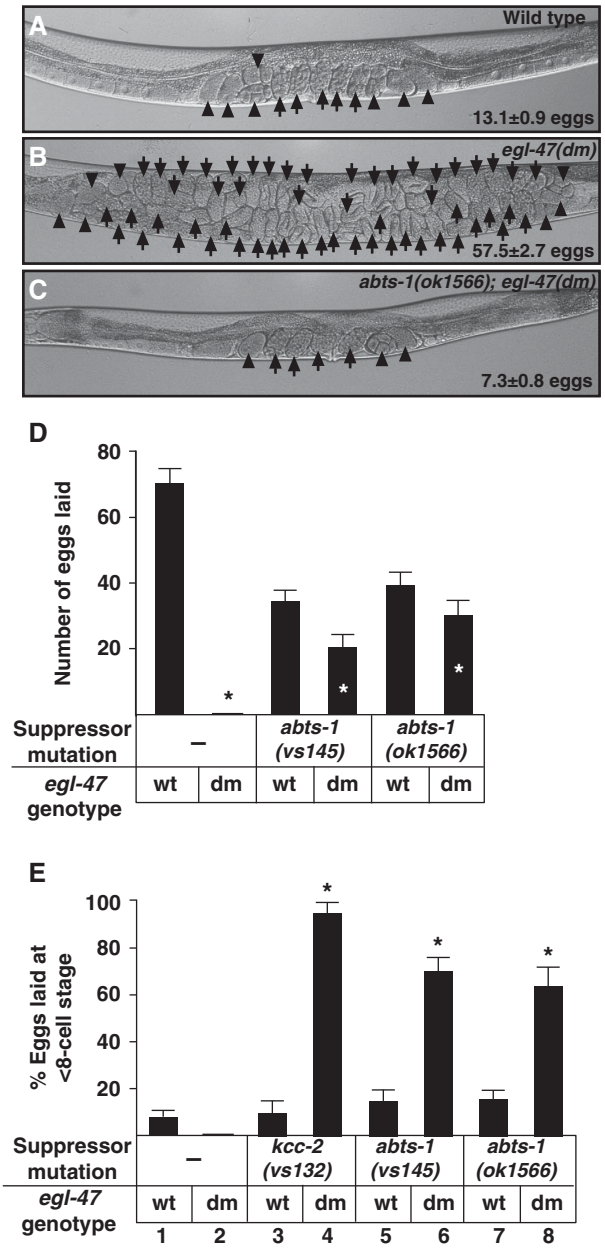

Figure 1 Mutations in *abts-1* suppress the *egl-47(dm)* egg-laying defect. (**A**–**C**) Representative images of wild-type, *egl-47(dm)*, and *abts-1(ok1566); egl-47(dm)* worms. The average number of unlaid eggs is shown (±95% confidence interval). $n \geqslant 30$ animals for each genotype. Eggs with eight or fewer cells (arrowheads) and eggs with more than eight cells (arrows). (**D**) Eggs laid by pools of five young adult worms, by 18 h after the late-L4 stage. Wild-type young adults lay many eggs, while *egl-47(dm)* young adults never lay any eggs. Mutations in *abts-1* significantly suppress the *egl-47(dm)* egg-laying defect ($P < 0.005$; comparing bars with white asterisks to the black asterisked control with zero eggs). For each genotype $n = 6$ pools of five worms each. Error bars in this and subsequent figures represent standard errors except when otherwise noted. (**E**) Proportion of eggs laid at an early developmental stage. Wild-type (bar 1), *egl-47(dm)* (bar 2), *abts-1(vs145)* (bar 3), *abts-1(ok1566)* (bar 5), and *kcc-2(vs132)* (bar 7) animals all lay a low proportion of early-stage eggs that have not yet reached the eight-cell stage. *abts-1(vs145); egl-47(dm)* (bar 4), *abts-1(ok1566); egl-47(dm)* (bar 6), and *kcc-2(vs132); egl-47(dm)* (bar 8) animals all lay a high proportion of such early-stage eggs (asterisks indicate $P < 0.05$ compared with the bar 2 control). $n \geqslant 100$ eggs for each genotype, error bars show the 95% confidence interval. These results show that *egl-47(dm)* significantly stimulates egg laying in the absence of ABTS-1 or KCC-2.

©2011 European Molecular Biology Organization

To assay for an increased rate of egg laying, we measured the developmental stage of freshly laid eggs. *C. elegans* eggs are fertilized internally and undergo cell divisions *in utero* prior to being laid. In wild-type animals only ~5% of freshly laid eggs are at an early developmental stage (defined as eight cells or fewer). Mutants that lay eggs at a higher rate than do wild-type animals retain eggs *in utero* for a shorter period of time and thus lay a higher percentage of their eggs at an early developmental stage (Chase and Koelle, 2004). Using this assay, we found that while wild-type animals, *egl-47(dm)* mutants, and *abts-1* single mutants lay a low percentage of early-stage eggs, *abts-1; egl-47(dm)* double mutants lay over 60% of their eggs at an early developmental stage (Figure 1E). Thus, *abts-1* mutations, like *kcc-2* mutations, reverse the effect of *egl-47(dm)* on egg laying, but do not change egg-laying behaviour in the absence of *egl-47(dm)* or other challenges to the egg-laying system. *abts-1* mutants lay fewer cumulative eggs than do wild-type animals (Figures 1C and 4), but this observation can be attributed to decreased egg production in *abts-1* mutants (Supplementary Figure S1), an effect that is also observed in *kcc-2* mutants (Tanis *et al*, 2009).

ABTS-1 is a Na^+-driven chloride–bicarbonate exchanger

To analyse ABTS-1 function, we used *Xenopus* oocytes to express the ABTS-1 protein and monitored membrane ion transport using intracellular ion-selective microelectrodes (Figure 2). Previous experiments with the ABTS-1 'B' isoform (isoforms are shown in Figure 3A) revealed that it functioned as an electroneutral Na^+/HCO_3^- cotransporter (Romero and Boron, 1998). However, this early study did not address the potential role of Cl^-, as the transport activity was quite low. Studies of the ABTS-1 'A' isoform indicated that it functions as a Cl^-–HCO_3^- exchanger, but did not address any potential role of Na^+ (Sherman *et al*, 2005). In the present study, we sought to more fully characterize the transport properties of ABTS-1, specifically to determine whether it is an NDAE that acts to extrude Cl^-.

We found that the transport activity of ABTS-1 is consistent with Na^+-driven Cl^-–HCO_3^- exchange. The ion transport activity by ABTS-1 is somewhat lower than that of many other HCO_3^- transporters (note differences in the magnitude of pH change in Figure 2Ab and Bb), complicating some measures of its transport activity. We therefore tested the hypothesis that ABTS-1 is an NDAE by directly comparing ABTS-1 activity (Figure 2A) to that of a known Na^+-driven Cl^-–HCO_3^- exchanger, *Drosophila* NDAE1 (Figure 2B). Water-injected control oocytes had minimal background transport activity (Figure 2C). ABTS-1 (Figure 2A) and NDAE1 (Figure 2B) expression resulted in HCO_3^- transport (measured with intracellular pH microelectrodes) in response to removal

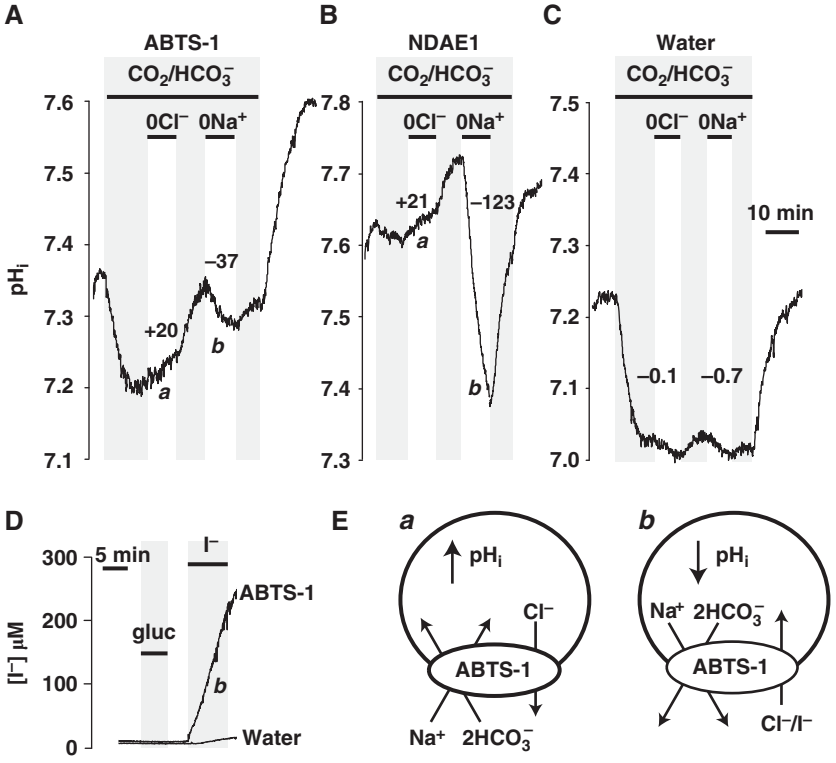

Figure 2 ABTS-1 is a sodium-driven chloride–bicarbonate exchanger. (**A**–**C**) Electrophysiology data from pH microelectrodes in *Xenopus* oocytes. In the presence of 1.5% CO_2/10 mM HCO_3^- (pH 7.5), both ABTS-1 (**A**) and *Drosophila* NDAE1 (**B**) responded to Cl^- replacement ($0Cl^-$) by increasing pH_i (HCO_3^- influx to oocyte), while water-injected oocytes (**C**) showed no response. By contrast, Na^+ removal ($0\ Na^+$) resulted in dramatic pH_i decreases (HCO_3^- efflux from oocyte) in oocytes expressing ABTS-1 (**A**) and NDAE1 (**B**), while water-injected oocytes (**C**) showed no response. Rates of alkalinization during Cl^- and Na^+ removal (# $\times 10^{-5}$ pH units/s) are indicated above the respective segments of the pH_i traces. (**D**) Electrophysiology data from halide microelectrodes in *Xenopus* oocytes. In oocytes expressing ABTS-1 and water-injected controls, replacement of extracellular Cl^- with gluconate produced no change in $[Cl^-]$. When extracellular Cl^- was replaced by I^-, the electrode sensed I^- influx in oocytes expressing ABTS-1, but not in water-injected controls. (**E**) Models illustrating the suggested transport activity of ABTS-1 and NDAE1 in response to removal of extracellular Cl^- (a) and in response to removal of extracellular Na^+ or addition of extracellular I^- (b). The transport activity illustrated in panel (**E**a) is also the predicted activity of ABTS-1 under normal conditions. The stoichiometry shown, with two HCO_3^- ions transported, is consistent with the observed electroneutrality of the transport.

 ©2011 European Molecular Biology Organization

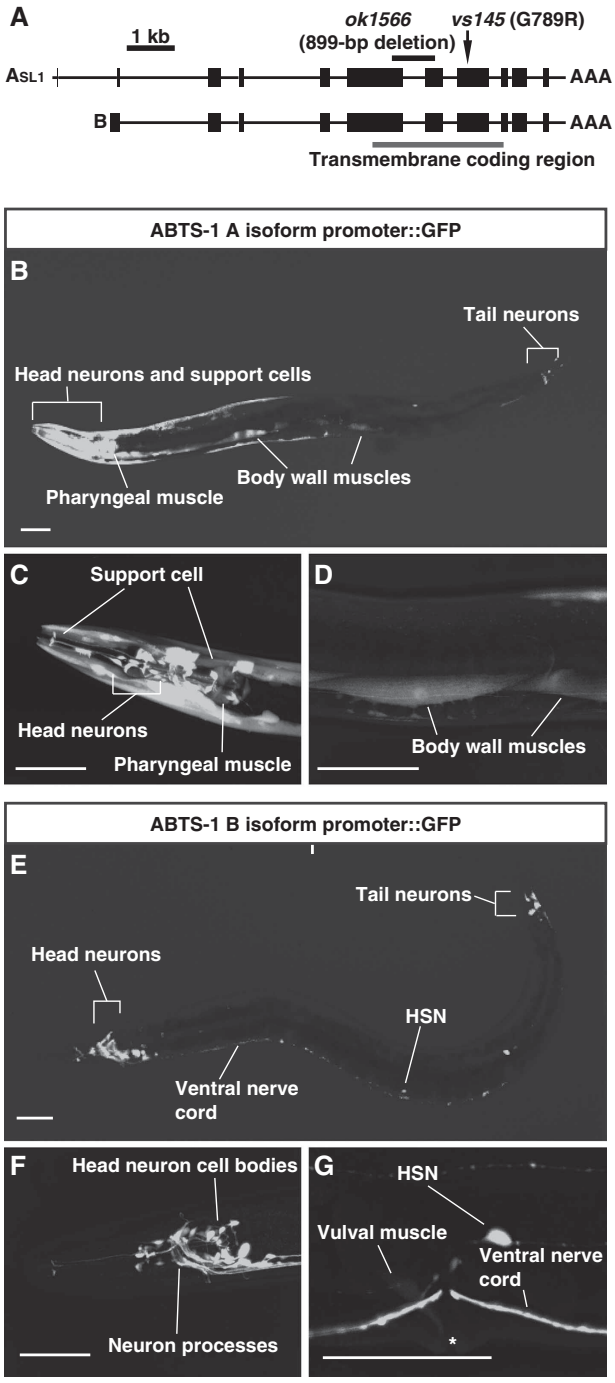

Figure 3 ABTS-1 is expressed predominantly in neurons and muscles. (**A**) The gene structure of *abts-1*. Two *abts-1* transcripts, *abts-1a* and *abts-1b*, have different start sites that splice onto common exons. Black bars represent exons and connecting lines indicate introns. Indicated are the polyadenylation site (AAA) and the SL1 *trans* splice leader (SL1). Also displayed are the transmembrane domain coding region (grey bar) and the locations of the *vs145* point mutation and the *ok1566* deletion mutation. (**B–D**) GFP fluorescence in animals carrying an *abts-1a* promoter::*gfp*::*abts-1* 3′ UTR reporter transgene. This reporter transgene was expressed in many cells including the BWMs, pharyngeal muscles, and head and tail neurons. (**E–G**) GFP fluorescence in animals carrying an *abts-1b* promoter::*gfp*::*abts-1* 3′ UTR reporter transgene. This reporter transgene was expressed primarily in neurons, including the HSN, and in the vulval muscles. Scale bars in all images are 50 μm.

of Cl^- or Na^+. With Cl^- removal (0 Cl^-) both ABTS-1 and NDAE1 produced an increase of intracellular pH (pH_i), indicating HCO_3^- movement into the cell (model in Figure 2Ea). This response is characteristic of Cl^-–HCO_3^- exchange (Romero *et al*, 2000; Chang *et al*, 2009). Next, we removed Na^+ (0 Na^+). Both ABTS-1 and NDAE1 responded by decreasing pH_i, indicating HCO_3^- movement out of the cell (model in Figure 2Eb). This effect is consistent with Na^+-driven Cl^-–HCO_3^- exchange (Romero *et al*, 2000; Grichtchenko *et al*, 2001). Monitoring of V_m indicated that this transport activity was electroneutral (Supplementary Figures S2 and S3).

Many Cl^- transport systems will also transport other halides (e.g. I^- and Br^-). The order of preference of halides (the Hoffmeister series) may be used to distinguish anion transport systems (Wright and Diamond, 1977). Figure 2D shows that ABTS-1 expression provided *Xenopus* oocytes with I^- transport activity. By calibrating our anion-sensitive microelectrodes (see Materials and methods), we determined that for ABTS-1-expressing *oocytes* incubated in high extracellular [I^-], intracellular [I^-] reached ∼250 μM within 5 minutes. In contrast, intracellular [I^-] did not increase in control oocytes injected with water rather than ABTS-1 copy RNA (cRNA) (Figure 2D). The model in Figure 2Eb represents the proposed transport mechanism that occurs during Na^+ removal (Figure 2A) and during I^- addition (Figure 2D): ABTS-1 transports Na^+ and HCO_3^- out of the cell while transporting halides into the cell.

ABTS-1 is broadly expressed in C. elegans neurons and muscles

C. elegans KCC-2 is expressed in excitable cells such as neurons and muscles where it presumably extrudes Cl^- to support inhibitory neurotransmission by ligand-gated Cl^- channels (Tanis *et al*, 2009). We observed a similar pattern of ABTS-1 expression. To examine the expression pattern of ABTS-1, we constructed *abts-1* promoter::*gfp*::*abts-1* 3′ UTR reporter transgenes in which GFP expression was driven by 5′ promoter and 3′ untranslated region sequences. Because the available ABTS-1 cDNAs showed the presence of two transcripts with different 5′ exons (Figure 3A), we generated two reporter constructs using the promoter regions for each of the two isoforms (Supplementary Figure S4). We found that the *abts-1a* promoter drove expression of GFP in head, tail, and lateral neurons as well as in BWMs, pharyngeal muscles, and neural support cells (Figure 3B–D). The *abts-1b* promoter drove expression of GFP in head neurons, tail neurons, and the HSNs, as well as weak expression in the vulval muscles (Figure 3E–G).

ABTS-1 is required for UNC-49-mediated inhibition of egg laying

Given the apparently similar mutant phenotypes, Cl^- extrusion activities, and expression patterns of ABTS-1 and KCC-2, we hypothesized that ABTS-1 may have a similar role to KCC-2 in establishing the cellular Cl^- gradient that supports the inhibitory action of GABA-gated Cl^- channels. UNC-49 is the *C. elegans* $GABA_A$ receptor homologue, and its function is dependent on KCC-2 (Bamber *et al*, 1999; Tanis *et al*, 2009). The $GABA_A$ receptor agonist muscimol is a potent inhibitor of egg laying in wild-type animals, but not in animals that have compromised UNC-49 function. Thus, muscimol does not

©2011 European Molecular Biology Organization

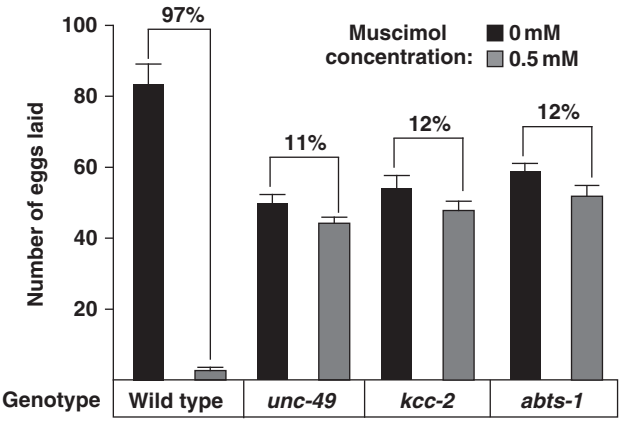

Figure 4 ABTS-1 is required for the inhibition of egg-laying behaviour by muscimol. The average number of eggs laid by pools of five animals over 2 h in the presence or absence of 0.5 mM muscimol. *unc-49*, *kcc-2*, and *abts-1* mutants were all resistant to the inhibitory effects of muscimol on egg-laying behaviour. Brackets indicate the percent inhibition by muscimol. For each genotype $n = 6$ pools of five worms each.

inhibit egg laying in animals lacking UNC-49 or in animals lacking KCC-2 (Tanis *et al*, 2009).

We found that muscimol also fails to inhibit egg laying in *abts-1* mutants. In control wild-type animals, muscimol inhibited egg laying by 97%: over 2 h, pools of five animals laid 83.5 ± 5.6 eggs in the absence but only 2.7 ± 0.9 eggs in the presence of muscimol (Figure 4A). This effect requires UNC-49 and KCC-2, since the corresponding mutants showed only 11 and 12% inhibition of egg laying by muscimol, respectively (Figure 4A). Similarly, we found that the *abts-1* mutant showed only 12% inhibition of egg laying by muscimol (Figure 4A). Thus, ABTS-1 may function similarly to KCC-2 in generating the Cl^- gradient required for muscimol to inhibit egg laying via UNC-49.

Inhibition of egg laying by muscimol requires KCC-2 function in the HSNs (Tanis *et al*, 2009). We found that ABTS-1 function is also required in the HSNs for normal sensitivity to muscimol. The inhibitory effect of muscimol on egg laying was partially restored by re-expression of ABTS-1 in the HSNs of *abts-1* mutants as compared with *abts-1* mutants expressing a GFP control protein (Supplementary Figure S5). The fact that re-expression of ABTS-1 only partially rescued muscimol sensitivity may indicate that ABTS-1 function is required in an additional cell type or that our transgene drives expression of ABTS-1 in the HSNs at a sub-wild-type level. We also observed that re-expression of ABTS-1 in the HSNs of the *abts-1; egl-47(dm)* mutant rescued the *egl-47(dm)* egg-laying defect (Supplementary Figure S6), providing additional evidence for ABTS-1 function in the HSNs.

UNC-49 activation excites rather than inhibits BWMs in the absence of ABTS-1

While GABA is normally an inhibitory neurotransmitter, neurons that do not have a mechanism to extrude Cl^- may have relatively high intracellular Cl^- levels that lead to an excitatory effect of $GABA_A$ receptor activation (Kaneko *et al*, 2004). Such an effect is observed in *C. elegans* BWMs, which receive inputs from GABAergic motor neurons that act to inhibit and lengthen the BWMs during the animal's locomotion (McIntire *et al*, 1993b). While wild-type animals exposed to muscimol undergo simultaneous relaxation of all BWMs and thus an increase in total body length, *kcc-2* mutants experience muscle contraction and shortening of total body length (Tanis *et al*, 2009). The standard electrophysiological method for assaying changes in Cl^- reversal potential (Blaesse *et al*, 2009) appears not to work on *C. elegans* muscle cells due to the failure of the ionophore gramicidin to perforate the membranes of these cells (data not shown). Nevertheless, the behavioural response to muscimol strongly suggest that there is a depolarizing shift in the Cl^- reversal potential in the muscles of *kcc-2* mutants, resulting in an excitatory effect of UNC-49 activation.

We found that *abts-1* mutants exposed to muscimol undergo a decrease in body length similar to that observed in *kcc-2* mutants. Wild-type animals exposed to muscimol experienced a significant increase in body length from $1207 \pm 6\,\mu m$ before exposure to $1277 \pm 9\,\mu m$ after exposure (Figure 5A, B, and E). In contrast, the *abts-1* mutant underwent a significant decrease in body length when exposed to muscimol from $1021 \pm 7\,\mu m$ before exposure to $984 \pm 8\,\mu m$ following exposure (Figure 5C–E). This shortening effect was comparable to that observed in *kcc-2* mutants (Figure 5E). Both the lengthening observed in wild-type animals and the shortening observed in *abts-1* and *kcc-2* mutants were dependent on the UNC-49, as loss of UNC-49 function in any genetic background resulted in no change in body length following muscimol exposure (Figure 5E).

KCC-2 and UNC-49 both function in the BWMs to mediate the effect of muscimol on body length (Tanis *et al*, 2009), and we found that ABTS-1 also functions in the muscles to control this effect of muscimol. Wild-type and *abts-1* mutant animals expressing the control protein GFP in their BWMs showed lengthening and shortening in response to muscimol, respectively, comparable to that observed in non-transgenic wild-type and *abts-1* mutant animals (Figure 5F). Re-expression of ABTS-1 in the muscles of *abts-1* mutants converted their muscimol response from shortening back to a lengthening similar to that seen in the wild-type controls (Figure 5F).

These results are consistent with a model in which ABTS-1 acts as a Cl^- extruder in the BWMs, along with KCC-2, to help set the cellular Cl^- gradient required for UNC-49-mediated inhibition (Figure 5G) and muscle lengthening. In this model, loss of ABTS-1 or KCC-2 function results in accumulation of intracellular Cl^- and thus a depolarizing shift in the Cl^- reversal potential to produce UNC-49-mediated excitation and muscle contraction (Figure 5H).

ABTS-1 and KCC-2 function redundantly in the BWMs to mediate endogenous inhibitory GABA signalling

Mutants that lack UNC-49 display sluggish and uncoordinated locomotion (McIntire *et al*, 1993a; Bamber *et al*, 1999). Despite the fact that *abts-1* and *kcc-2* mutants show excitatory rather than inhibitory responses to the $GABA_A$ agonist muscimol, these mutants still show well-coordinated locomotion (Supplementary Videos S1, S2, S3, and S4). One model suggested by these observations is that modest changes in the cellular Cl^- gradient produced by loss of one transporter do reverse the flow of Cl^- through the UNC-49 Cl^- channel, but the low levels of UNC-49 activation caused by endogenous, synaptically released GABA still result in 'shunting'

 ©2011 European Molecular Biology Organization

inhibition of the muscles to allow coordinated movement (see the Discussion for further elaboration of this model).

The model that ABTS-1 and KCC-2 act in parallel predicts that a mutant lacking both ABTS-1 and KCC-2 would show phenotypic defects more severe than the relatively mild defects observed in *abts-1* or *kcc-2* single mutants. We found that the *abts-1; kcc-2* double mutant indeed has severe defects in muscle contractility and locomotion not observed in either single mutant. We measured the body length of animals not exposed to any drug and found that wild-type body length was 1212 ± 6 μm, and the body lengths of *abts-1* and *kcc-2* mutants were modestly shorter at 1064 ± 8 μm and 1145 ± 6 μm respectively (Figure 6A, B, C, and E). The *unc-49* mutant was also modestly shorter than wild-type animals (Figure 6E). The modest shortening in all these mutants was presumably due to increased BWM contraction. However, the *abts-1; kcc-2* double mutant exhibited a much more severe body-length defect, as these animals were only 510 ± 10 μm long (Figure 6D and E).

The *abts-1; kcc-2* double mutant also exhibited severe locomotion defects. We counted the number of body bends executed over a 1-min period and found that wild-type animals and *kcc-2* mutants performed a similar number of coordinated body bends, while *abts-1* mutants performed a lower number (Figure 6F; Supplementary Videos S1, S3, and S4) The *unc-49* mutant executed even fewer body bends (Figure 6F), and these body bends were not coordinated (Supplementary Video S2), presumably due to lack of normal muscle relaxation. The *abts-1; kcc-2* double mutant executed almost no body bends and was essentially incapable of locomotion (Figure 6F; Supplementary Video S5).

Both the double-mutant body-length and locomotion defects described above presumably result from BWM hypercontraction, and we performed cell-specific rescue experiments to demonstrate that re-expression of either ABTS-1 or KCC-2 in the BWMs is sufficient to at least partially rescue each of these defects. Double-mutant animals carrying a control transgene driving GFP expression in the BWMs exhibited similar body lengths to the non-transgenic animals described above (compare Figure 6E and G) and were never capable of coordinated locomotion (Supplementary Video S6). However, *abts-1; kcc-2* mutant animals carrying transgenes driving expression of either ABTS-1 or KCC-2 in the BWMs displayed significant rescue of the *abts-1; kcc-2*

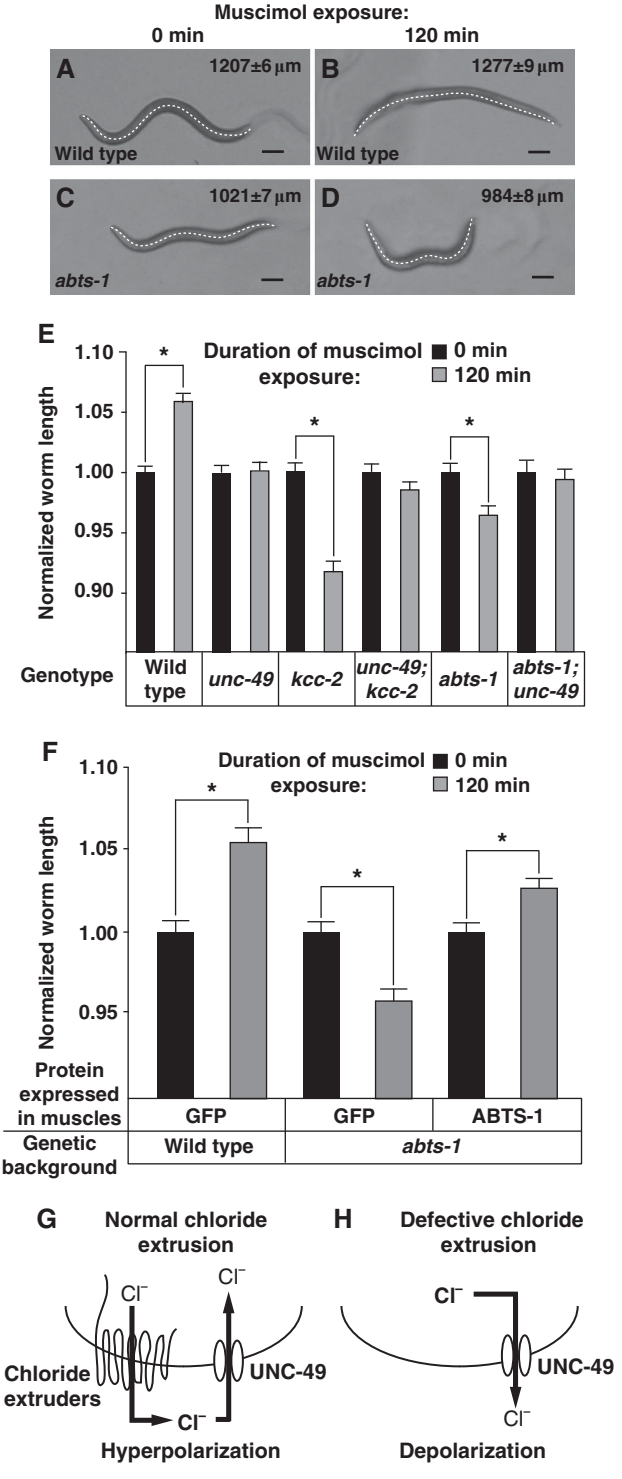

Figure 5 ABTS-1 is required for the inhibition of muscle contraction by muscimol. (**A**, **B**) Images of representative wild-type animals in the absence (**A**) or presence (**B**) of 1 mM muscimol. A line was drawn down the centre of each worm image as indicated to measure body length. Average lengths ± standard errors are shown for each condition. $n \geqslant 30$ animals for each genotype. Scale bars = 100 μm. (**C**, **D**) Images of representative *abts-1* animals in the absence (**C**) or presence (**D**) of 1 mM muscimol. (**E**) Average body length before and after 2 h of exposure to 1 mM muscimol. Wild-type animals displayed significant increases in body length following muscimol exposure, while *abts-1* and *kcc-2* mutants displayed significant decreases. Strains with *unc-49* mutations showed no changes in body length. For each genotype, body-length measurements were normalized to body length prior to muscimol exposure. $n \geqslant 30$ animals for each genotype. Asterisks indicate significant changes with $P < 0.005$. (**F**) Average body length of transgenic animals before and after 2 h of exposure to 1 mM muscimol. A muscle-specific promoter was used to transgenically express cDNAs encoding the control protein GFP or ABTS-1. Re-expression of ABTS-1 in the BWMs of *abts-1* mutants caused a significant increase in body length following muscimol exposure, in contrast to the muscimol-induced shortening observed in *abts-1* mutants expressing GFP in the BWMs. $n \geqslant 50$ animals for each genotype. Asterisks are as in panel (**E**). (**G**) Model depicting that Cl^--extruding transporters establish a gradient of Cl^- ions across the membrane such that the Cl^- reversal potential is more negative than the membrane resting potential. Thus, UNC-49 activation leads to Cl^- influx and hyperpolarization. (**H**) Model depicting that cells not expressing Cl^--extruding transporters maintain relatively high intracellular Cl^- levels such that the Cl^- reversal potential is more positive than the resting potential. Thus, UNC-49 activation leads to Cl^- efflux and depolarization.

©2011 European Molecular Biology Organization

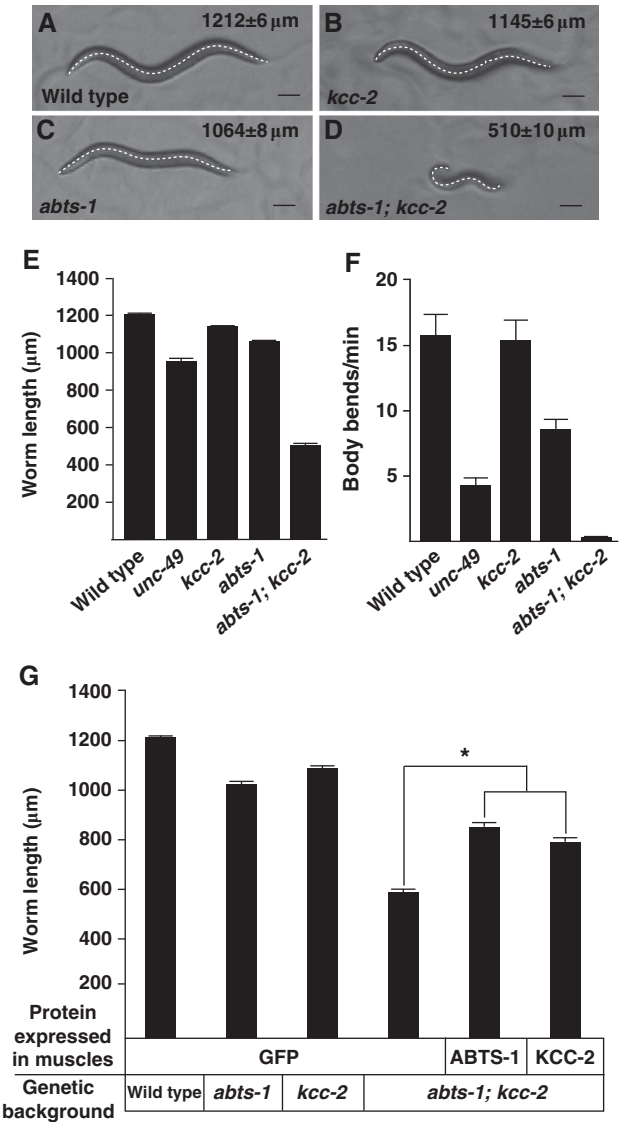

Figure 6 ABTS-1 and KCC-2 function redundantly in the BWMs to mediate muscle inhibition and relaxation. (**A**–**D**) Images of representative wild-type and mutant animals. Genotypes for each worm are indicated. A line was drawn down the centre of each worm image as indicated to measure body length. Average lengths ± standard errors are shown for each condition. Scale bars = 100 μm. (**E**) Average body length of wild-type and mutant animals. Mutants defective in muscimol responsiveness were slightly shorter than wild-type animals. The *abts-1; kcc-2* double mutant was dramatically shorter than wild-type animals. $n \geqslant 15$ animals for each genotype. (**F**) Average number of body bends executed by wild-type and mutant animals in a 1-min period. Body bends were moderately reduced in *abts-1* mutants, more severely reduced in *unc-49* mutants, and almost completely absent in *abts-1; kcc-2* double mutants. $n \geqslant 30$ animals for each genotype (see also Supplementary Movies S1–S7). (**G**) Average body length of muscle-rescued transgenic animals. A muscle-specific promoter was used to transgenically express cDNAs encoding the control protein GFP, ABTS-1, or KCC-2. Re-expression of ABTS-1 or KCC-2 in the muscles partially rescued the body-length defect of the *abts-1; kcc-2* double mutant. $n \geqslant 30$ animals for each genotype.

body-length defect (Figure 6G), and often showed well-coordinated movement (Supplementary Video S7). These results are consistent with a model in which ABTS-1 and KCC-2 act in parallel in the BWMs to extrude Cl^- and in which loss of both transporters results in muscle hypercontraction that produces dramatic defects in body length and in locomotion.

Mutations that eliminate GABAergic transmission reduce the severity of the *abts-1; kcc-2* double-mutant phenotype, consistent with a model in which excitatory GABA signalling contributes to this phenotype. The body lengths of *abts-1; unc-49; kcc-2* and *abts-1; unc-25; kcc-2* triple mutants (*unc-25* encodes the GABA biosynthetic enzyme glutamic acid decarboxylase) are slightly, but significantly, longer than *abts-1; kcc-2* double mutants (Supplementary Figure S7). The fact that mutations in *unc-49* and *unc-25* only partially ameliorate the *abts-1; kcc-2* phenotype suggests that chloride conductances in addition to those of UNC-49 are disrupted in *abts-1; kcc-2* double mutants.

Transcriptional regulation of ABTS-1 and KCC-2 expression are coordinately controlled

In mammalian brain, expression of *Kcc2* is transcriptionally upregulated during the late stages of neuronal development, and this is associated with a negative shift in the Cl^- reversal potential that converts the effect of GABA from excitatory to inhibitory (Rivera *et al*, 1999; Ben-Ari, 2002). In *C. elegans*, KCC-2 expression is transcriptionally upregulated in the HSNs during the transition from larva to adult (Tanis *et al*, 2009), coinciding with the timing of HSN synapse formation (Adler *et al*, 2006; Ding *et al*, 2007).

We examined expression of GFP from an *abts-1* transcriptional reporter transgene during development. We first examined the HSNs, as the development of these neurons is especially well characterized (Desai *et al*, 1988; Adler *et al*, 2006; Ding *et al*, 2007). The *abts-1b* promoter::*gfp*::*abts-1* 3′ UTR reporter transgene drives GFP expression in the HSNs of transgenic animals and is the only *abts-1* isoform-reporter that does so (Figure 3). Thus, we measured GFP fluorescence levels in the HSNs of L3- and L4-stage larval and adult transgenic animals carrying the *abts-1b* reporter. GFP fluorescence was generally not seen in the HSNs of L3 animals (Figure 7A and I). GFP was reliably expressed at a low level in L4 transgenic animals (Figure 7B and I), and there was an additional 3.7-fold increase in GFP fluorescence in the HSNs of adult animals as compared with L4 animals (Figure 7C and I). Although the upregulation of GFP expression is seen with both *abts-1* and *kcc-2* reporter transgenes (Tanis *et al*, 2009), it is not a property of all transgenes that drive GFP expression in the HSN: an *unc-86* promoter::*gfp* transgene drives strong GFP expression in the HSNs in L3, L4, and adult stages (Figure 7D, E, F, and J). Additionally, the upregulation of *abts-1* appears to be associated with neuronal maturation, not the transition from larva to adult, as similar levels of GFP expression in the BDU neuron, which matures early in embryonic development (Walthall and Chalfie, 1988), were observed at the larval and adult time points tested (Figure 7K).

We observed that *abts-1::gfp* expression was significantly increased in the HSNs of *kcc-2* mutants (Figure 7G, H, and L). There was a 2.3-fold increase in GFP fluorescence in the HSNs of *kcc-2* mutants as compared with wild-type animals. This result suggests that *abts-1* expression may be upregulated to compensate for loss of KCC-2 function. In contrast, *kcc-2* promoter::*gfp* expression in the HSNs of animals was not significantly altered in *abts-1* mutant as compared with wild-type animals (data not shown), so such compensation was not seen in reverse.

 ©2011 European Molecular Biology Organization

Discussion

ABTS-1 and KCC-2 function partially redundantly to mediate inhibitory GABA signalling

Our results suggest that ABTS-1 and KCC-2 function partially redundantly. Each transporter is required in the HSNs for the inhibition of egg laying by EGL-47(dm), a putative transmembrane receptor whose ligand and precise mechanism of inhibiting neural activity remain unidentified. ABTS-1 and KCC-2 are also required in the HSN neurons for inhibition of egg-laying behaviour by the GABA receptor agonist muscimol. In addition to the HSNs, ABTS-1 and KCC-2 also function in the BWMs to mediate the inhibitory effects of muscimol on muscle contraction. Muscimol activates the $GABA_A$ receptor UNC-49 in wild-type animals to produce muscle lengthening and increased body length. However, the *abts-1* and *kcc-2* mutations reverse the effects of muscimol so that body shortening is observed. Analogously, *abts-1* and *kcc-2* mutations reverse the effect of the *egl-47(dm)* mutation so that it strongly stimulates rather than inhibits egg laying, strongly suggesting that the unknown mechanism of neural inhibition by EGL-47 involves the activation of a chloride conductance. While the *abts-1* and *kcc-2* single mutants display remarkably similar effects when challenged by the *egl-47(dm)* mutation or muscimol, neither transporter mutant shows strong behavioural defects in the absence of these challenges. However, we found that the *abts-1; kcc-2* double mutant displays severe defects in body length and locomotion attributable at least in part to lack of inhibitory GABA signalling onto BWMs. Consistent with our hypothesis that ABTS-1 is required for proper inhibition of BWMs, Liao *et al* (2010) recently observed that *abts-1* mutants are hypersensitive to an acetylcholine agonist that stimulates BWM contraction. Taken together, these observations strongly suggest that ABTS-1 and KCC-2 function partially redundantly to mediate inhibition of neurons and muscles.

Our work suggests that the redundant function shared by KCC-2 and ABTS-1 is Cl^- extrusion, and that ABTS-1 is as important as KCC-2 in controlling the cellular Cl^-gradient. We have characterized the transport activities of KCC-2 (Tanis *et al*, 2009) and ABTS-1, and their only shared ion transport activity is the ability to extrude intracellular Cl^-. Past studies of neuronal Cl^- extrusion have focused on the KCCs (Blaesse *et al*, 2009). NDAEs such as ABTS-1, which use Na^+ influx to drive Cl^-–HCO_3^- exchange resulting in Cl^- extrusion and increased intracellular pH, have been previously cloned and characterized in invertebrate and mammalian systems (Romero *et al*, 2000; Grichtchenko *et al*, 2001; Virkki *et al*, 2003). Despite the Cl^--extrusion of these transporters, they have been studied and discussed mainly in the context of

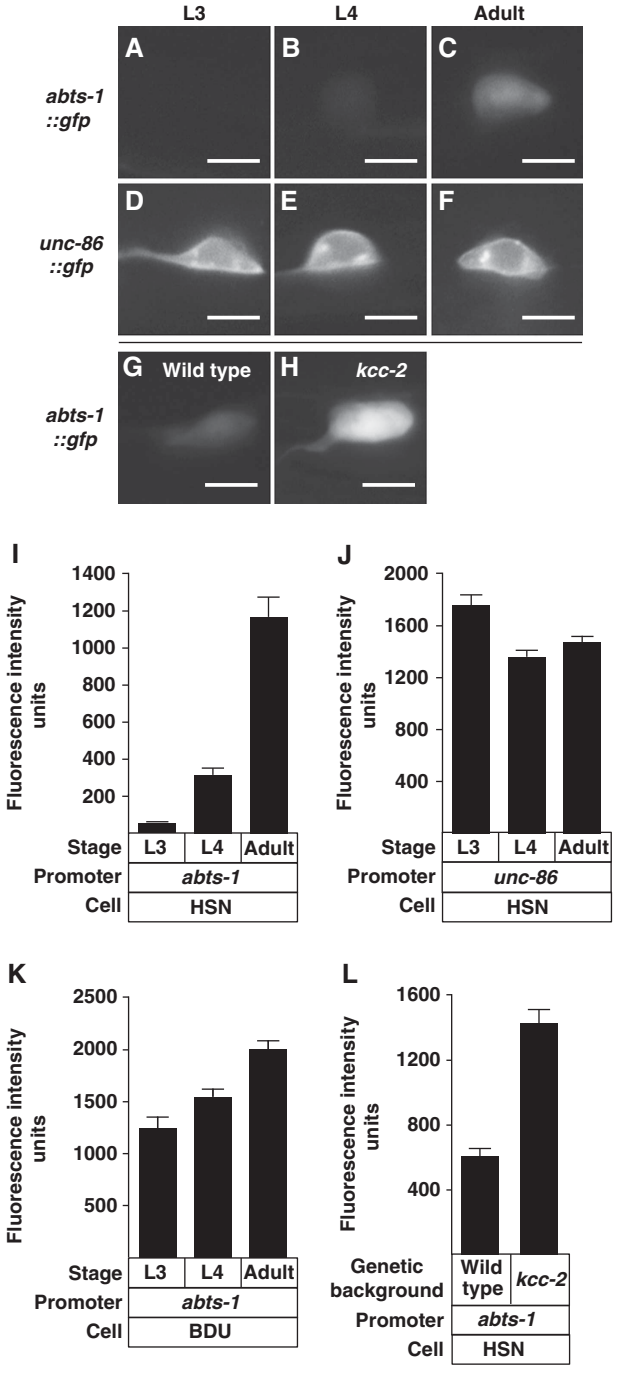

Figure 7 Expression of *abts-1* in the HSNs is upregulated during neuronal maturation and synapse formation. (**A–C**) Images of representative HSNs at three stages of development expressing GFP from the *abts-1b* promoter::*gfp*::*abts-1* 3′ UTR transgene. (**D–F**) Images of representative HSNs at three stages of development expressing GFP from the *unc-86* promoter::*gfp* transgene. (**G**, **H**) Images of representative HSNs of wild-type and *kcc-2* mutant animals (as indicated by white text) expressing GFP from the *abts-1b* promoter::*gfp* ::*abts-1* 3′ UTR transgene. Scale bars in panels (**A–H**) = 5 μm. (**I**) Mean GFP fluorescence of the HSN cell body in animals at three stages of development carrying the *abts-1b* promoter::*gfp*::*abts-1* 3′ UTR reporter transgene. GFP fluorescence increased from barely detectable to strong between the L3 and adult stages. For each stage $n \geqslant 30$ cell bodies. (**J**) Mean GFP fluorescence of the HSN cell body in animals at three stages of development carrying the *unc-86* promoter::*gfp* reporter transgene. GFP was highly expressed at all developmental stages analysed. For each stage $n \geqslant 30$ cell bodies. (**K**) Mean GFP fluorescence of the BDU cell body in larval and adult animals carrying the *abts-1b* promoter::*gfp*::*abts-1* 3′ UTR reporter transgene. GFP was highly expressed at all developmental stages analysed. For each stage $n \geqslant 30$ cell bodies. (**L**) Mean GFP fluorescence of the HSN cell body in wild-type and *kcc-2* mutant animals carrying the *abts-1b* promoter::*gfp*::*abts-1* 3′ UTR reporter transgene. Expression of the reporter is increased in the HSNs of *kcc-2* mutants as compared with wild-type animals. For each stage $n \geqslant 30$ cell bodies. In panels (**I–L**) different exposure settings were used to capture images for analysis in each panel. Thus, arbitrary fluorescence units cannot be compared across experiments.

©2011 European Molecular Biology Organization

cellular pH regulation (Schwiening and Boron, 1994; Baxter and Church, 1996). ABTS-1 presumably regulates BWM pH *in vivo* by coupling Cl^- extrusion to HCO_3^- import. The HCO_3^- content of the extracellular space surrounding the BWMs is unknown, but the BWMs do express the carbonic anhydrase, CAH-4, which may act a source of HCO_3^- for ABTS-1 transport (Hall *et al*, 2008). Thus, it is possible that ABTS-1 controls muscle contractility through its pH regulatory function. However, intracellular acidification, the expected result of loss of ABTS-1 function, is associated with loss of muscle contractility (Westerblad *et al*, 1998), which is the opposite of the *abts-1* mutant phenotype. Our results suggest that mutants for KCC-2, the principal KCC of *C. elegans* neurons and muscles (Tanis *et al*, 2009), are only partially defective for cellular Cl^- extrusion, that mutants for ABTS-1 are about as defective for this function as are mutants for KCC-2, and that profound defects in Cl^- extrusion are only seen in double mutants lacking both transporters. These results imply that a principle physiological function of NDAEs is to control the cellular Cl^- gradient and that further analysis of NDAEs will provide a more complete understanding of Cl^- extrusion from excitable cells.

The relationship between KCC-2 and ABTS-1 function is revealed by single and double mutants for these transporters. High levels of Cl^- extrusion in the wild type produce a steep cellular Cl^- gradient such that opening of $GABA_A$ channels results in Cl^- influx and hyperpolarization. Partial loss of Cl^- extrusion, such as may occur in *kcc-2* or *abts-1* single mutants, could reduce the Cl^- gradient such that the Cl^- reversal potential is more positive than the cell's resting potential and opening of Cl^- channels results instead in Cl^- efflux. Given these results, it might appear puzzling that although the normal inhibitory signalling through UNC-49 is required for coordinated locomotion in *C. elegans* (McIntire *et al*, 1993a), *kcc-2* and *abts-1* single mutants still show coordinated locomotion. We propose that in these mutants, the relatively weak $GABA_A$ activation produced by endogenous synaptic GABA release results in shunting inhibition, a phenomenon in which the $GABA_A$-mediated current effectively short-circuits excitation by tending to prevent depolarization beyond the Cl^- reversal potential to the more positive levels needed to excite the cell (Farrant and Kaila, 2007). Consistent with this idea, previous work has shown that, at certain Cl^- reversal potentials, weak $GABA_A$ activation can be inhibitory while massive and prolonged $GABA_A$ activation can become excitatory by setting the resting potential to a more positive level (Kaila, 1994). Finally, our model proposes that in *absts-1; kcc-2* double mutants, lack of any Cl^- extrusion function and the likely presence of an NKCC (Figure 8) could result in intracellular Cl^- accumulation, and the reversed Cl^- gradient produced would cause even relatively weak synaptic GABA release to result in strong depolarization and excitation. This would explain the hypercontracted muscles and uncoordinated locomotion observed in the double transporter mutants.

Implications for understanding control of neural excitability in the mammalian brain

In the mammalian brain, NDAEs are likely to provide a Cl^- extrusion function analogous to that of ABTS-1. Gulacsi *et al* (2003) observed that dopaminergic neurons in the rat substantia nigra do not express KCC2, but still exhibit inhibitory responses to GABA that are dependent upon the presence of extracellular HCO_3^-. More recently, glycinergic neurons of the brainstem have been shown to exhibit activity-dependent negative shifts in Cl^- reversal potential that are dependent upon extracellular HCO_3^- and are blocked by inhibitors of SLC4 transporters (Kim and Trussell, 2009). A candidate for the transporter mediating these effects is the Na^+-driven Cl^-–HCO_3^- exchanger (NDCBE) encoded by *slc4a8* (Kim and Trussell, 2009), which has well-characterized electroneutral Na^+-driven Cl^-–HCO_3^- exchange activity (likely Na^+:$2HCO_3^-$ exchange for Cl^-) and is expressed in mammalian neurons (Grichtchenko *et al*, 2001; Chen *et al*, 2008a, b). However, a role for NDCBE in controlling inhibitory neurotransmission has not been unambiguously demonstrated, as previous studies (Gulacsi *et al*, 2003; Kim and Trussell, 2009) have inhibited Na^+-driven Cl^-–HCO_3^- exchange with manipulations that would be expected to affect all brain-expressed SLC4 family members, only some of which are NDAEs. Thus, our study is the first to specifically inactivate an NDAE and demonstrate its role in controlling inhibitory GABA signalling.

A role for NDAEs in regulating GABA signalling may explain the relationship between pH and neural excitability in the mammalian brain. KCCs function primarily as Cl^- extruders, whereas NDAEs both extrude Cl^- and have an additional role, via HCO_3^- influx, in intracellular alkalinization

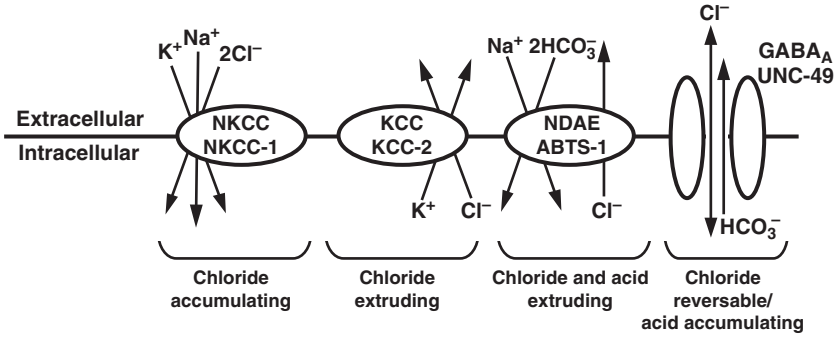

Figure 8 Schematic of ion fluxes mediated by NKCCs, KCCs, NDAEs, and $GABA_A$ receptors. NKCCs mediate Cl^- influx driven by the cellular Na^+ gradient, while KCCs mediate Cl^- efflux driven by the K^+ gradient. NDAEs mediate Cl^- efflux and acid extrusion (HCO_3^- influx driven by the cellular Na^+ gradient). $GABA_A$ receptors are anion channels that allow Cl^- and HCO_3^- ions across the membrane, with the direction of flow dictated principally by the ion concentration gradients produced by the three types of transporters diagrammed. Designations for both mammalian and *C. elegans* homologues of each protein are indicated.

 ©2011 European Molecular Biology Organization

(Figure 8). NDAEs are activated by intracellular acidification (Schwiening and Boron, 1994), suggesting that regulation of the Cl^- gradient by NDAEs may be closely tied to regulation of cellular pH. Neuronal acidification may be induced by prolonged firing (reviewed by Chesler, 2003), by efflux of HCO_3^- through $GABA_A$ receptors (Kaila and Voipio, 1987; Pasternack *et al*, 1993), or during pathological states such as epileptic seizures (Somjen, 1984). In each case, activation of NDAEs by acidification may help to maintain a hyperpolarized Cl^- reversal potential and thus promote the inhibitory action of GABA. Acidification of the brain is known to be associated with termination of seizure activity (Xiong *et al*, 2000). We propose that activation of NDAEs by acidosis may also contribute to seizure termination by promoting a more negative Cl^- reversal potential and thus promoting the inhibitory effects of GABA. Consistent with the hypothesis that NDAEs use activity-dependent acidosis to control the Cl^- reversal potential, Kim and Trussell (2009) have shown that prolonged spiking drives intracellular acidification that, in turn, leads to negative shifts in the Cl^- reversal potential that require SLC4 transport activity. Additionally, mutations that disrupt the putative human NDAE gene *slc4a10* are associated with epilepsy (Gurnett *et al*, 2008), a finding that is consistent with an antileptic activity of NDAEs.

Transcriptional regulation of Cl^--extruding transporter expression regulates inhibitory neurotransmission

Our demonstration that multiple Cl^--extruding transporters generate the cellular Cl^- gradient suggests that a cell's response to inhibitory neurotransmitters is shaped by the combination of Cl^- extruders that it expresses. Both ABTS-1 and KCC-2 (Tanis *et al*, 2009) are expressed in the HSNs and BWMs and both contribute to inhibitory neurotransmission in these cells. Some cells however express only ABTS-1 or KCC-2, such as the ventral cord motor neurons, which express only KCC-2. This observation may explain the fact that *kcc-2* mutants are resistant to paralysis by exogenous serotonin (Tanis *et al*, 2009), while *abts-1* mutants are not (data not shown), as the paralytic effects of serotonin are mediated in part by the serotonin-gated Cl^- channel MOD-1, which is expressed in ventral cord motor neurons (Ranganathan *et al*, 2000).

The demonstration that expression of *abts-1* is upregulated during the maturation of the HSNs coincident with upregulation of *kcc-2* expression and synapse formation suggests that maturation of the cellular Cl^- gradient and responses to inhibitory neurotransmitter involves the coordinated upregulation of these two transporters. Studies in mammals have focused on the upregulation of KCC2 expression and also the coincident downregulation of NKCC1 expression as the driving forces behind the maturation of the cellular Cl^- gradient and inhibitory GABA signalling (Rivera *et al*, 1999; Yamada *et al*, 2004; Romero *et al*, 2009). No comprehensive analysis of SLC4 transporter expression in the nervous system across development has been completed, although NDCBE is detected in the choroid plexus of embryonic rats (Chen *et al*, 2008a) and throughout the brain of early postnatal mice (Chen *et al*, 2008b). Our work suggests that developmental regulation of these transporters may participate in fine-tuning the cellular Cl^- gradient during development to produce mature neurons that exhibit proper inhibitory neurotransmission and electrical excitability.

We found that transcription from the *abts-1* promoter is upregulated in the HSNs of adult *kcc-2* mutants. This suggests that transcription of these transporters is regulated dynamically in the adult nervous system, potentially in response to changes in either the intracellular $[Cl^-]$ or electrical excitability. This extends the concept of ionic plasticity (Rivera *et al*, 2005) to one in which excitable cells have the ability to monitor and adjust levels of inhibitory neurotransmission through continuous adjustment Cl^- transporter expression to alter of intracellular Cl^- levels.

Materials and methods

C. elegans strains

All strains used in this work are detailed in the Supplementary data.

Transgenes

Transgenic strains were constructed by injection of plasmid DNA or PCR products into the germline (Mello *et al*, 1991). We constructed *abts-1* promoter::*gfp*::*abts-1* 3′ UTR plasmids for the *abts-1a* (pAB9A) and *abts-1b* (pAB36A) promoters. PCR-amplified promoter::*gfp*::3′ UTR cassettes from these plasmids were injected (Etchberger and Hobert, 2008). For analysis of developmental changes in *abts-1b* expression (Figure 7), the extrachromosomal array containing *abts-1b* promoter::*gfp*::3′ UTR reporter transgene was chromosomally integrated using psoralen/UV mutagenesis. The resulting integrated strains were outcrossed at least four times. The *unc-86* promoter::*gfp* transgene was as described previously (Adler *et al*, 2006).

The HSN cell-specific rescue plasmid (pAB11A) was obtained by inserting the *abts-1a* cDNA into an HSN expression vector (Tanis *et al*, 2008). A construct used to express GFP in the HSNs (pJM60A) and an empty HSN vector (pJM66A) were used as controls. The HSN cell-specific rescue construct was injected with pJM60A and the coinjection marker *myo-2::gfp* (pJKL449.1) (Huang and Stern, 2004) into LX1320 *abts-1(ok1566)*. Wild-type animals and LX1320 were injected with pJM60A, pJM66A, and pJKL449.1 to generate transgenic control strains. The muscle cell-specific rescue plasmid (pAB23A) was generated by inserting the *abts-1a* cDNA into the pPD96.52 vector that drives muscle expression using the *myo-3* promoter (Reynolds *et al*, 2005). A *myo-3*::*gfp* construct (pAB25A) was used as a control and a construct expressing nuclear-localized GFP in the muscles (pSAK2) was used as a coinjection marker (Fire *et al*, 1998). Wild-type and LX1320 animals were injected with pAB25A and pSAK2 to generate control strains. LX1320 animals were injected with pAB23A and pSAK2 to generate muscle-rescued strains.

Details of all transgenes and plasmids used in this work are described in the Supplementary data.

Behavioural assays

Animals for behavioural assays were picked at the late-fourth larval (L4) stage, a time point about 6 h prior to adulthood. Animals were assayed as adults after 24 h (Figures 4–6) or 30 h (Figure 1A, B, C, and E) of incubation at 20°C. Suppression of *egl-47(dm)* (Figure 1D) was assayed by measuring the number of eggs laid by pools of five worms over 18 h after staging as late-L4s. Unlaid eggs and early-stage eggs were measured as described by Chase and Koelle (2004). Muscimol inhibition of egg laying was assayed as previously described (Tanis *et al*, 2009). At least six plates carrying five worms each were assayed per genotype (Figure 4A). For cell-specific rescue experiments, at least two plates carrying five worms each from each of five transgenic lines were assayed (Supplementary Figure S5).

Muscimol-induced changes in body length were measured as described by Tanis *et al* (2009). For non-transgenic wild-type and mutant animals, at least 30 animals were analysed per genotype (Figure 5E). For experiments testing cell-specific rescue of the *abts-1* muscimol sensitivity defect, at least 10 animals for each of five transgenic lines were analysed (Figure 5F). Body lengths of non-drug-exposed animals were also measured using this method. At least 15 animals were analysed per genotype (Figure 6E). In experiments testing cell-specific rescue of the *abts-1; kcc-2*

©2011 European Molecular Biology Organization

mutant phenotype, at least 30 animals from one transgenic line was analysed for each strain (Figure 6G).

Body bends (Figure 6F) were measured as described by Chase and Koelle (2004). At least 30 animals were assayed per genotype, for 1 min each.

Microscopy

Animals were immobilized for microscopy on agar pads with 10 mM levamisole. Transgenic animals containing *abts-1* reporter transgenes imaged with a Zeiss LSM 510 confocal microscope and reconstructed using Volocity software (Improvision). For analysis of changes in *abts-1* and *unc-86* expression during development and in the *kcc-2* mutant background, images were obtained using a Carl Zeiss Axioskop. Single images through a central focal plane of the left HSN cell body were acquired for each animal, and mean GFP intensity for the area of the entire cell body was calculated for each HSN using Openlab software (Improvision). Developmental age was scored using distal tip cell migration for L3 larvae and vulval morphology for L4 larvae. Adult animals were staged 12 h after the late-L4 stage. At least 30 animals were analysed per developmental stage and genotype.

Xenopus oocyte expression and electrophysiology

The coding sequence for ABTS-1a was subcloned into the *Xenopus* oocyte expression vector pGEMHE. ABTS-1 and NDAE1 cRNA was synthesized *in vitro* using the T7 mMessage mMachine (Ambion, Austin, TX). Stage V/VI oocytes were isolated by limited collagenase digestion (Romero *et al*, 1998). Oocytes were injected with 25 ng cRNA in 50 nl (0.5 μg/μl) or 50 nl RNAse-free water. Oocytes were studied 3–7 days after injection in a perfusion chamber and monitoring pH_i, $[Cl^-]_i$, and V_m as previously (Romero *et al*, 2000; Kato *et al*, 2009). Oocytes were perfused with ND96 (96 mM NaCl, 2 mM KCl, 1.8 mM $CaCl_2$, 1.0 mM $MgCl_2$ and 5 mM HEPES, pH 7.5, 195 ± 5 mOsm). The 1.5% CO_2/10 mM HCO_3^- solution replaced 10 mM NaCl with 10 mM $NaHCO_3$ but maintained pH 7.5 (Romero *et al*, 2000). Recordings shown in Figure 2 are each representative of results from 4 to 6 oocytes.

Since changes in intracellular $[Cl^-]$ were not obvious, we monitored $[I^-]$ using a halide-sensitive microelectrode. This approach greatly increases the signal-to-noise ratio as free $[I^-]$ is typically <1 μM in most vertebrate cells. Iodide calibration was performed for each electrode by varying $[I^-]$ between 100 μM and 10 mM (NaI) in a background of 40 mM NaCl (resting $[Cl^-]$ in these ABTS-1 oocytes). This approach documented the offset for 100 μM I^- in a constant $[Cl^-]$ background. The I^--specific electrode slope was then determined between 100 μM and 10 mM NaI.

Supplementary data

Supplementary data are available at *The EMBO Journal* Online (http://www.embojournal.org).

Acknowledgements

We thank the *Caenorhabditis* Genetics Center for strains, Keith Nehrke for the *abts-1* cDNA, and Bob Horvitz for sharing unpublished information about *abts-1*. This work was supported by NIH grants NS36918 (to MRK), DK056218 and EY017732 (to MFR), DK83007Z-02S2 (to TH), and NS060432 (to AB).

Conflict of interest

The authors declare that they have no conflict of interest.

References

Adler CE, Fetter RD, Bargmann CI (2006) UNC-6/Netrin induces neuronal asymmetry and defines the site of axon formation. *Nat Neurosci* **9:** 511–518

Akerman CJ, Cline HT (2006) Depolarizing GABAergic conductances regulate the balance of excitation to inhibition in the developing retinotectal circuit *in vivo*. *J Neurosci* **26:** 5117–5130

Bamber BA, Beg AA, Twyman RE, Jorgensen EM (1999) The *Caenorhabditis elegans* unc-49 locus encodes multiple subunits of a heteromultimeric GABA receptor. *J Neurosci* **19:** 5348–5359

Baxter KA, Church J (1996) Characterization of acid extrusion mechanisms in cultured fetal rat hippocampal neurones. *J Physiol* **493:** 457–470

Ben-Ari Y (2002) Excitatory actions of GABA during development: the nature of the nurture. *Nat Rev Neurosci* **3:** 728–739

Blaesse P, Airaksinen MS, Rivera C, Kaila K (2009) Cation-chloride cotransporters and neuronal function. *Neuron* **61:** 820–838

Chang MH, Plata C, Zandi-Nejad K, Sindic A, Sussman CR, Mercado A, Broumand V, Raghuram V, Mount DB, Romero MF (2009) Slc26A9 - anion exchanger, channel and Na^+ transporter. *J Membr Biol* **128:** 125–140

Chase DL, Koelle MR (2004) Genetic analysis of RGS protein function in *Caenorhabditis elegans*. *Methods Enzymol* **389:** 305–320

Chen LM, Kelly ML, Parker MD, Bouyer P, Gill HS, Felie JM, Davis BA, Boron WF (2008a) Expression and localization of Na-driven Cl-HCO(3)(-) exchanger (SLC4A8) in rodent CNS. *Neuroscience* **153:** 162–174

Chen LM, Haddad GG, Boron WF (2008b) Effects of chronic continuous hypoxia on the expression of SLC4A8 (NDCBE) in neonatal versus adult mouse brain. *Brain Res* **1238:** 85–92

Chesler M (2003) Regulation and modulation of pH in the brain. *Physiol Rev* **83:** 1183–1221

Desai C, Garriga G, McIntire SL, Horvitz HR (1988) A genetic pathway for the development of the *Caenorhabditis elegans* HSN motor neurons. *Nature* **336:** 638–646

Ding M, Chao D, Wang G, Shen K (2007) Spatial regulation of an E3 ubiquitin ligase directs selective synapse elimination. *Science* **317:** 947–951

Etchberger JF, Hobert O (2008) Vector-free DNA constructs improve transgene expression in *C. elegans*. *Nat Methods* **5:** 3

Farrant M, Kaila K (2007) The cellular, molecular, and ionic basis of $GABA_A$ receptor signaling. *Prog Brain Res* **160:** 59–87

Fire A, Xu S, Montgomery MK, Kostas SA, Driver SE, Mello CC (1998) Potent and specific genetic interference by double-stranded RNA in *Caenorhabditis elegans*. *Nature* **391:** 806–811

Fiumelli H, Cancedda L, Poo MM (2005) Modulation of GABAergic transmission by activity via postsynaptic Ca2+-dependent regulation of KCC2 function. *Neuron* **48:** 773–786

Grichtchenko II, Choi I, Zhong X, Bray-Ward P, Russell JM, Boron WF (2001) Cloning, characterization, and chromosol mapping of a human electroneutral Na^+-driven Cl-HCO_3^- exchanger. *J Biol Chem* **276:** 8358–8363

Gulacsi A, Lee CR, Sik A, Viitanen T, Kaila K, Tepper JM, Freund TF (2003) Cell type-specific differences in chloride-regulatory mechanisms and $GABA_A$ receptor-mediated inhibition in rat substantia nigra. *J Neurosci* **23:** 8237–8246

Gurnett CA, Veile R, Zempel J, Blackburn L, Lovett M, Bowcock A (2008) Disruption of sodium bicarbonate transporter SLC4A10 in a patient with complex partial epilepsy and mental retardation. *Arch Neurol* **65:** 550–553

Hall RA, Vullo D, Innocenti A, Scozzafava A, Supuran CT, Klappa P, Mühlschlegel FA (2008) External pH influences the transcriptional profile of the carbonic anhydrase, CAH-4b in *Caenorhabditis elegans*. *Mol Biochem Parasitol* **161:** 140–149

Huang P, Stern MJ (2004) FGF signaling functions in the hypodermis to regulate fluid balance in *C. elegans*. *Development* **131:** 2595–2604

Jorgensen EM (2005) GABA. In *WormBook*, The *C. elegans* Research Community (ed) WormBook, doi/10.1895/wormbook.1.14.1, http://www.wormbook.org

Kaila K, Voipio J (1987) Postsynaptic fall in intracellular pH induced by GABA-activated bicarbonate conductance. *Nature* **330:** 163–165

Kaila K (1994) Ionic basis of $GABA_A$ receptor channel function in the nervous system. *Prog Neurobiol* **42:** 489–537

Kaneko H, Putzier I, Frings S, Kaupp UB, Gensch T (2004) Chloride accumulation in mammalian olfactory sensory neurons. *J Neurosci* **24:** 7931–7938

 ©2011 European Molecular Biology Organization

Kato A, Kurita Y, Nakada T, Ogoshi M, Nakazato T, Doi H, Chang M-H, Hirose S, Romero MF (2009) Identification of renal transporters involved in sulfate excretion in marine teleost fish. *Am J Physiol Regul Integr Comp Physiol* **297:** R1647–R1659

Kim Y, Trussell LO (2009) Negative shift in the glycine reversal potential mediated by a Ca^{2+}- and pH-dependent mechanism in interneurons. *J Neurosci* **29:** 11495–11510

Liao VH, Liu JT, Li WT, Yu CW, Hsieh YC (2010) *Caenorhabditis elegans* bicarbonate transporter ABTS-1 is involved in arsenite toxicity and cholinergic signaling. *Chem Res Toxicol* **23:** 926–932

McIntire SL, Jorgensen E, Horvitz HR (1993a) Genes required for GABA function in *Caenorhabditis elegans*. *Nature* **364:** 334–337

McIntire SL, Jorgensen E, Kaplan J, Horvitz HR (1993b) The GABAergic nervous system of *Caenorhabditis elegans*. *Nature* **364:** 337–341

Mello CC, Kramer JM, Stinchcomb D, Ambros V (1991) Efficient gene transfer in *Celegans*: extrachromosomol maintenance and integration of transforming sequences. *EMBO J* **10:** 3959–3970

Mody I, De Koninck Y, Otis TS, Soltesz I (1994) Bridgeing the cleft at GABA synapses in the brain. *Trends Neurosci* **17:** 517–525

Moresco JJ, Koelle MR (2004) Activation of EGL-47, a $G\alpha_o$-coupled receptor, inhibits function of hermaphrodite-specific motor neurons to regulate *Caenorhabditis elegans* egg-laying behavior. *J Neurosci* **24:** 8522–8530

Pasternack M, Voipio J, Kaila K (1993) Intracellular carbonic anhydrase activity and its role in GABA-induced acidosis in isolated rat hippocampal pyramidal neurones. *Acta Physiol Scand* **148:** 229–231

Ranganathan R, Cannon SC, Horvitz HR (2000) MOD-1 is a serotonin-gated chloride channel that modulates locomotory behaviour in *C. elegans*. *Nature* **408:** 470–475

Reynolds NK, Schade MA, Miller KG (2005) Convergent, RIC-8-dependent Gα signaling pathways in the *Caenorhabditis elegans* synaptic signaling network. *Genetics* **169:** 651–670

Richmond JE, Jorgensen EM (1999) One GABA and two acetylcholine receptors function at the C. elegans neuromuscular junction. *Nat Neurosci* **2:** 791–797

Rivera C, Voipio J, Payne JA, Ruusuvuori E, Lahtinen H, Lamsa K, Pirvola U, Saarma M, Kaila K (1999) The K^+/Cl^- co-transporter KCC2 renders GABA hyperpolarizing during neuronal maturation. *Nature* **397:** 251–255

Rivera C, Voipio J, Kaila K (2005) Two developmental switches in GABAergic signalling: the K+-Cl- cotransporter KCC2 and carbonic anhydrase CAVII. *J Physiol* **562:** 27–36

Romero MF, Kanai Y, Gunshin H, Hediger MA (1998) Expression cloning using *Xenopus laevis* oocytes. *Methods Enzymol* **296:** 17–52

Romero MF, Boron WF (1998) Identification and expression of an electroneutral Na/HCO_3 cotransporter from *Caenorhabditis elegans* (ceNBC). *J Am Soc Nephrol* **9:** 11A

Romero MF, Henry D, Nelson S, Harte PJ, Dillon AK, Sciortino CM (2000) Cloning and characterization of a Na+-driven anion exchanger (NDAE1). A new bicarbonate transporter. *J Biol Chem* **275:** 24552–24559

Romero MF, Fulton CM, Boron WF (2004) The SLC4 family of HCO_3^- transporters. *Pflugers Arch* **447:** 495–509

Romero MF, Chang MH, Mount DB (2009) From cloning to structure, function, and regulation of chloride transporters. In *Physiology and Pathology of Chloride Transporters and Channels in the Nervous System: From Molecules to Diseases*, Alvarez-Leefmans FJ, Delpire E (eds) pp 43–80. Salt Lake City, UT: Elsevier Academic Press

Schwiening CJ, Boron WF (1994) Regulation of intracellular pH in pyramidal neurons from the rat hippocampus by Na^+-dependent Cl^-HCO3^- exchange. *J Physiol* **475:** 59–67

Sherman T, Chernova MV, Clark JS, Jiang L, Alper SL, Nehrke K (2005) The *abts* and *sulp* families of anion transporters from *Caenorhabditis elegans*. *J Physiol Cell Physiol* **289:** 341–351

Somjen GG (1984) Acidification of interstitial fluid in hippocampal formation caused by seizures and by spreading depression. *Brain Res* **331:** 186–188

Tanis JE, Moresco JJ, Lindquist RA, Koelle MR (2008) Regulation of serotonin biosynthesis by the G proteins $G\alpha_o$ and $G\alpha_q$ controls serotonin signaling in *Caenorhabditis elegans*. *Genetics* **178:** 157–169

Tanis JE, Bellemer A, Moresco JJ, Forbush B, Koelle MR (2009) The potassium chloride cotransporter KCC-2 coordinates development of inhibitory neurotransmission and synapse structure in *Caenorhabditis elegans*. *J Neurosci* **29:** 9943–9954

Virkki LV, Choi I, Davis BA, Boron WF (2003) Cloning of a Na^+-driven Cl/HCO3 exchanger from squid giant fiber lobe. *Am J Physiol Cell Physiol* **285:** C771–C780

Walthall WW, Chalfie M (1988) Cell-cell interactions in the guidance of late-developing neurons in *Caenorhabditis elegans*. *Science* **239:** 643–645

Westerblad H, Allen DG, Bruton JG, Allen DG, Andrade FH, Lännergren J (1998) Mechanisms underlying the reduction of isometric force in skeletal muscle fatigue. *Acta Physiol Scand* **162:** 253–260

Wright EM, Diamond JM (1977) Anion selectivity in biological systems. *Physiol Rev* **57:** 109–156

Xiong ZQ, Saggau P, Stringer JL (2000) Activity-dependent intracellular acidification correlates with the duration of seizure activity. *J Neurosci* **20:** 1290–1296

Yamada J, Okabe A, Toyoda H, Kilb W, Luhmann HJ, Fukuda A (2004) Cl^- uptake promoting depolarizing GABA actions in immature rat neocortical neurons is mediated by NKCC1. *J Physiol* **557:** 829–841

©2011 European Molecular Biology Organization